Primary Beam Corrections of MeerKAT Reference Pointed Data

W. D. Cotton (NRAO), September 22, 2023

***Abstract*—Alt-Az mounted radio antennas always have beam asymmetries which can cause imaging artifacts in interferometer arrays when these asymmetries cause variable gain in a given direction on the sky. If the detailed beam shape is known, it can, in principle, be corrected. This memo explores making beam corrections to reference pointed MeerKAT data. A comparison between the measured beam holography and a strong, weakly polarized calibrator viewed in a number of off–axis is presented. The results are baffling.**

***Index Terms*—Primary Beam Correction, Interoferometric Synthesis**

I. Introduction

THE dynamic range of images made with interferometer arrays can be limited by artifacts resulting from bright, off-axis sources being observed with antennas whose gain is a function of time with alt-az mounted antennas. These gain variations can arise from a number of effects including antenna mechanical mispointing and azimuthal asymmetries in the antenna gain pattern. Pointing errors can be greatly reduced using referenced pointing but antenna pattern effects need to be corrected during imaging using knowledge of the beam pattern.

Attempts to correct VLA data using holographically measured antenna patterns with varying degrees of success are reported in [1], [2]. The technique used in this memo is verified using simulated data as described in [3], [4], [5].

This memo describes an attempt to apply primary beam corrections using the Obit [6][1] package to reference pointed MeerKAT L band data. The holographically measured beam pattern of [7], [8] is used.

II. 14 June 2023 Reference Pointing Test

A test of reference pointing with MeerKAT at L band was performed on 14 June 2023 using the bright weakly polarized calibrator PKS0408-65. The observations occurred over 4 hours and antenna pointing errors were determined and corrected every 20 min. Cyclical observations were made with the calibrator on–axis and offset in the 4 cardinal directions, the pointing centers are given in Table I. The observations also included two scans on the polarized calibrator 3C138 (J0521+1638). The data were calibrated as described in [9]. For initial testing only Stokes I and no conversion to a circular basis was used. The data were divided into 8 Spectral windows (AKA IFs) for calibration purposes. In the nomenclature used the horizontal (H) feeds are referred to as "X" and the vertical (V) feeds as "Y".

TABLE I
14 June 2023 Pointing Offsets

Pointing	δRA °	δDec °
0408-65	0.0	0.0
J0400-6544	0.833433	-0.0133006
J0408-6635	0.0	0.8332818
J0416-6544	-0.833383	-0.0132995
J0408-6455	0.0	-0.8332472

The expectation is that the variations in antenna gain in the direction of PKS0408-65 in the offset positions is due to the variation of antenna gain with parallactic angle with time. It is also assumed that, after pointing corrections, all antennas will have approximately the same beam pattern. This expectation can be tested by comparing the observed visibilities with the average L band beam of [8].

A. Self Cal Gains

The observed antenna gains are most easily distilled by calibrating the pointing offset data using the image derived from the on–axis pointing. The calibration procedure derives the gain needed to correct the data so the estimate of the antenna gain is the inverse of the calibration gain. Figure 1 shows the one minute antenna averages of the parallel feeds, Spectral window 7 antenna gains for the J0400-6544 and J0408-6455 pointings with the one sigma variations as error bars. Plotted as a solid line are the interpolated antenna gain estimates from the holography beam maps at the frequency and beam location corresponding to the data-derived values.[2]

The ultimate test of making primary beam corrections is a reduction (or not) of the level of artifacts near bright sources. In order to make the comparison, the offset pointings were imaged in Stokes I using data in the linear basis with self calibration using Obit tasks MFBeam (makes beam corrections) and MFImage (no beam corrections). Phase self calibration was used for both imaging tasks and an additional amplitude and phase self cal for MFImage. CLEANing around the offset calibrator was restricted to nearby the source and the CLEAN

National Radio Astronomy Observatory, 520 Edgemont Rd., Charlottesville, VA, 22903 USA email: bcotton@nrao.edu

[1]http://www.cv.nrao.edu/∼bcotton/Obit.html

[2]The sign of the RA offset had to be negated to get agreement.

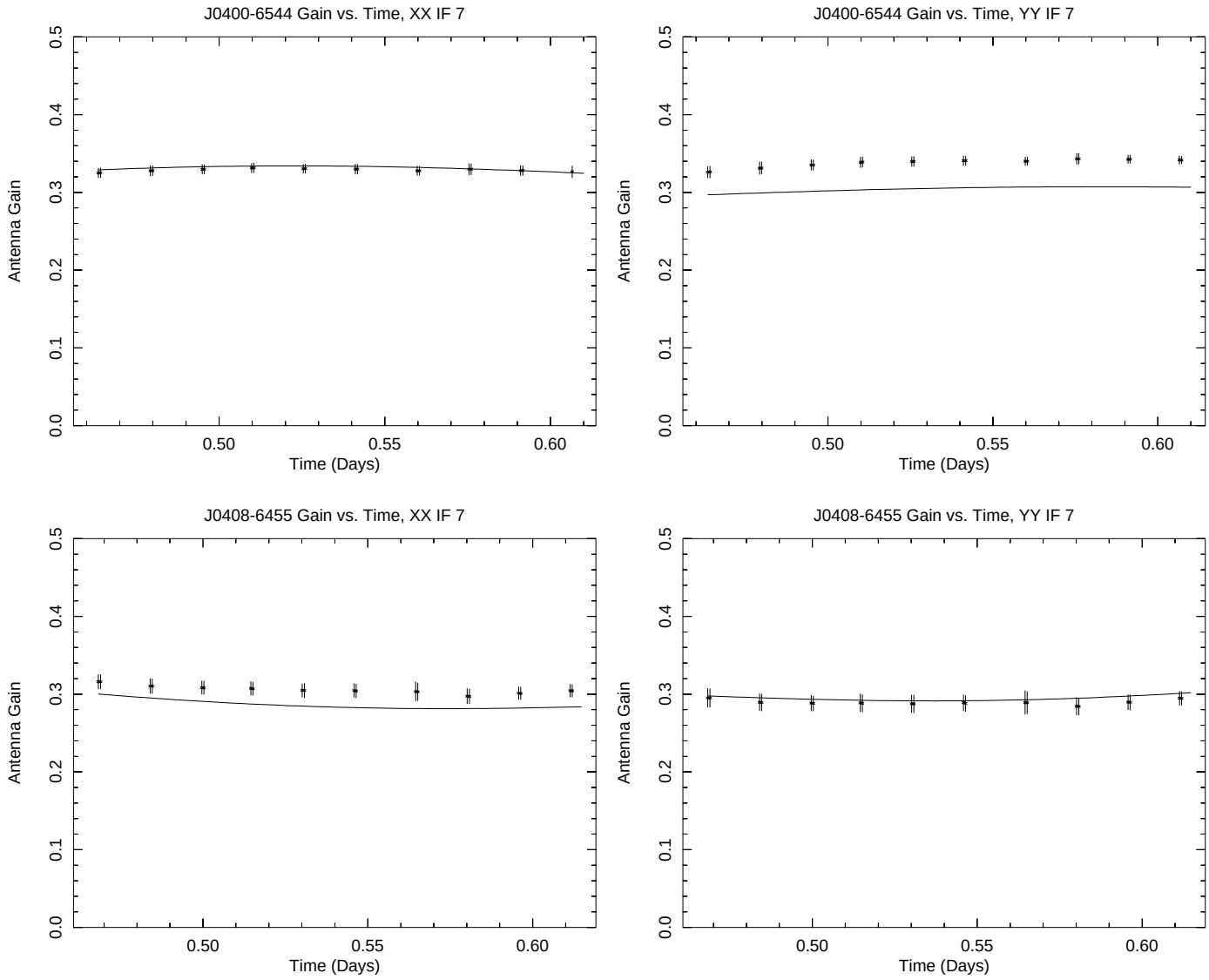

Fig. 1. Gains for Spectral Window 7 visibilities for two pointings. Stars ("*") are one min averages of antenna gains from calibrating the offset pointing data using the on–axis CLEAN model; error bars show the ±one sigma scatter. The solid line is Mattieu de Villiers's antenna beam model [8] interpolated to the corresponding beam location and frequency.
Top Left: J0400-6544 X
Top Right: J0400-6544 Y
Bottom Left: J0408-6455 X
Bottom Right: J0408-6455 Y

components were not restored to the final image. This allows a comparison of the various methods.

The expectation is that most variations in gain amplitude are due to beam asymmetries and variations in phase are due to the atmosphere and are removed by the phase calibration. This comparison is shown for pointing J0400-6544 in Figure 2 and for pointing J0408-6455 in Figure 3.

For pointing J0400-6544, the two phase self calibrated results are comparable and the amplitude and phase selfcalibrated data gives a somewhat lower level of artifacts. For pointing J0408-6455 applying the beam corrections resulted in a higher level of artifacts than either of the uncorrected versions. A curious feature is that in all cases the residuals are dominated by components that neither the beam corrections nor amplitude self calibration significantly reduced. This means that the artifacts are dominated by effects that are not simple time dependent antenna gain in the direction of the bright source.

B. Averaged Visibility Gains

An alternate method of estimating the gains is to average the data over baseline and channel in a spectral window and normalize by the total intensity in that spectral window. The technique for averaging over baseline with a shift in phase tracking center is described in [10] and is implemented in ObitTask AvgBL. The various offset pointings averaged over baseline and in 30 second spectral window segments and

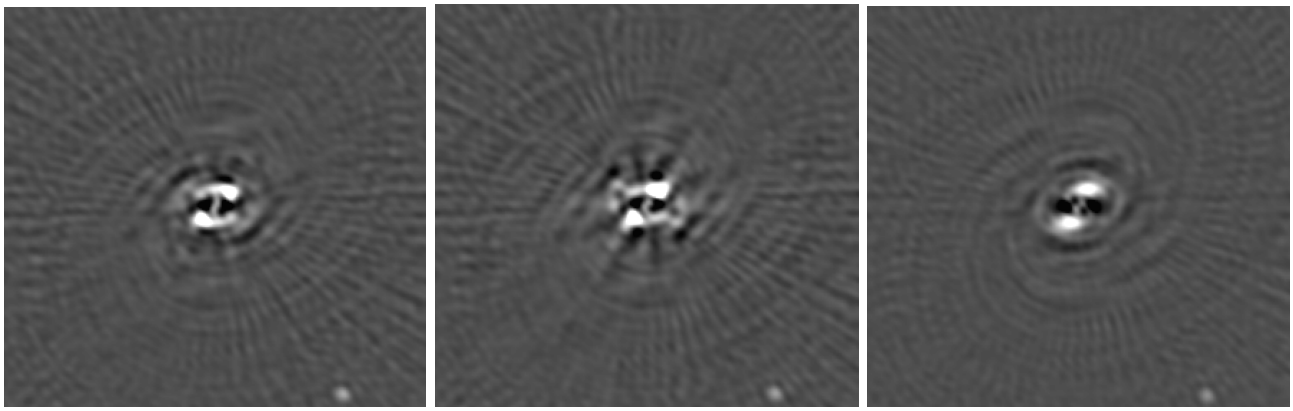

Fig. 2. Residual images of 0408-65 in the J0400-6544 pointing. The field of view is 5.9' × 5.6' and the range of pixel values is -3 to +7 mJy/bm. The CLEAN was not allowed to remove components away from the central response.
Left: MFBeam with phase self cal,
Middle: MFImage with phase self cal,
Right: MFImage with amp & phase self cal.

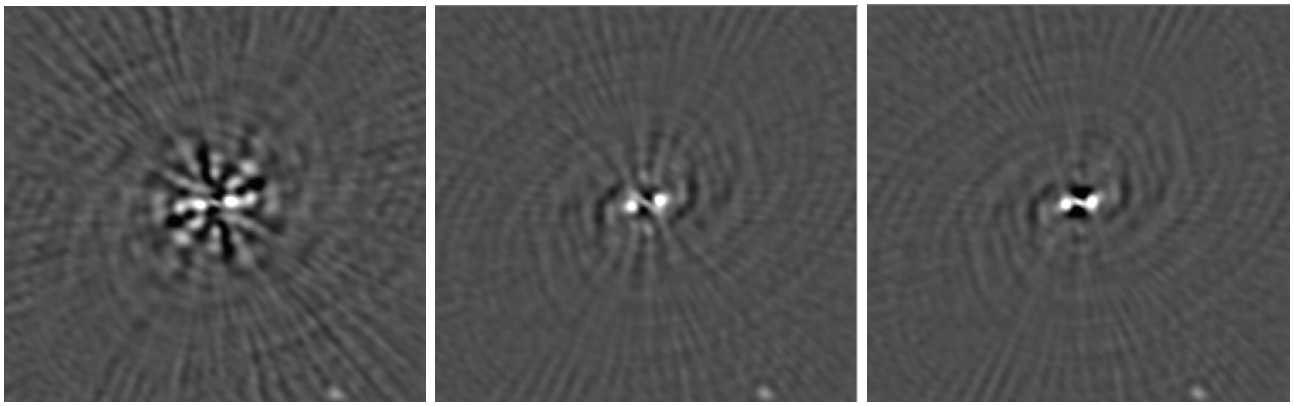

Fig. 3. Like Figure 2 but for the J0408-6455 pointing.
Left: MFBeam with phase self cal,
Middle: MFImage with phase self cal,
Right: MFImage with amp & phase self cal.

normalized by the total Stokes I flux density of PKS0408-65 for Spectral windows (IFs) 2 and 7 are shown in Figures 4 and 5. These Spectral windows sample near the bottom and top of the bandpass while avoiding bandedge effects. All pointings are included on the same plot with the parallactic angle plotted including the pointing offset. Thus, they show the location on the beam pattern being sampled.

An alternate way of looking at the data samples is interms of the equivalent Stokes parameters instead of the correlations. Figure 6 shows the Stokes visibilities for IF 2 normalized by the on–axis Stokes I flux density. This figure shows that the effect can largely be represented as Stokes parameters; the real part of these visibilities is substantially larger than the imaginary part, i.e. the phases are close to 0/180°.

There are significant differences in the gains derived from averaging the data and from the beam holography. The gains estimated from the cross polarized visibilities also have much higher absolute values than the beam holography. This could be due to some actual polarization of the calibrator; the polarization of other sources in the field should largely be rejected by the synthesis properties of the average over baseline. There will be some instrumental polarization as this data has not had the polarization calibration applied. However, the off-axis instrumental polarization should also be visible in the holography results.

Several results stand out:

1) The observed imaginary part of the parallel hand data are all much closer to zero, and more constant, than those from the holography beam. This means that the phases were close to zero. These data were not self calibrated, which would set the phases as close to zero as possible, but were calibrated using PKS0408-65 in the on–axis pointings. The antenna gain phases should cancel out if gain x gain* is used but this seems not to be the case for the holography beams.
2) There is no constant shift in parallactic angle that gets the observed visibilities to line up with the holography beams. The real part of the parallel hand (XX,YY) data cover similar ranges and have similar shapes with parallactic angle in both the observed data and the holography beam but not at the parallactic angle assigned to each.

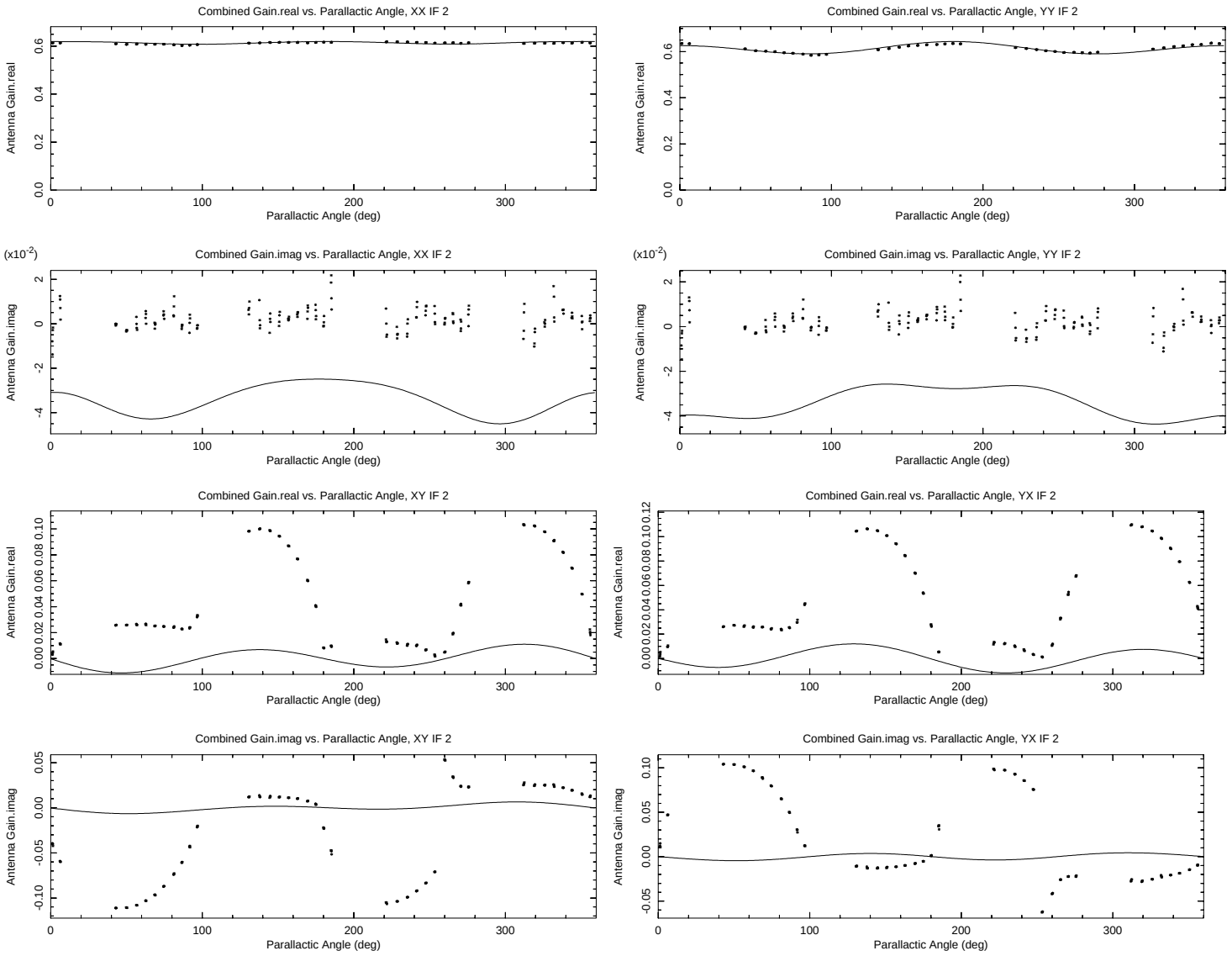

Fig. 4. XX,YY,XY and YX gains for Spectral Window 2 visibilities for all pointings. Stars (“*”) are 30 sec averages of visibilities over baseline and channel, normalised by the on–axis flux density. Parallactic angles of data points are adjusted to include the effect of the direction of the position offset The solid line is Mattieu de Villiers’s antenna beam model [8] interpolated to the corresponding beam location and frequency.
Upper panel real, lower imaginary.
Top Left: XX
Top Right: YY
Bottom Left: XY
Bottom Right: YX

C. Polarization Calibrated Data

In a test to see if the result above was adversely affected by the on–axis instrumental polarization, the test was repeated using polarization calibrated data.[3] The comparison of the calibrated data and the holography beams for spectral window IF 2 is shown in Figure 7. All pointings are included on the same plot with the parallactic angle plotted including the pointing offset.

In this test, spectral window IF 2 was chosen to minimize the off–axis instrument contribution while avoiding band–edge effects. This figure shows cross–hand data averages substantially in excess of the values from the holography beam. To test for low level calibrator polarization, the calibrated data for the on–axis observations of 0408-65 were imaged in I, Q, U and V; the linear polarization results are shown in Figure 8. This plot shows plausible linear polarization at a level of approximately 0.1% with a rotation measure of -0.60 $\pm$ 0.02. The Stokes V is even weaker, 0.0012% at the position of the calibrator and 0.0018% RMS in a 51×51 box centered on the calibrator.

The equivalent representation in terms of the normalized Stokes parameters is shown in Figure 9. The correlations are dominated by Stokes I and Q.

[3]In order to do this, the Obit calibration software was modified to allow writing calibrated data in the linear basis (XX,YY,XY,YX) [11].

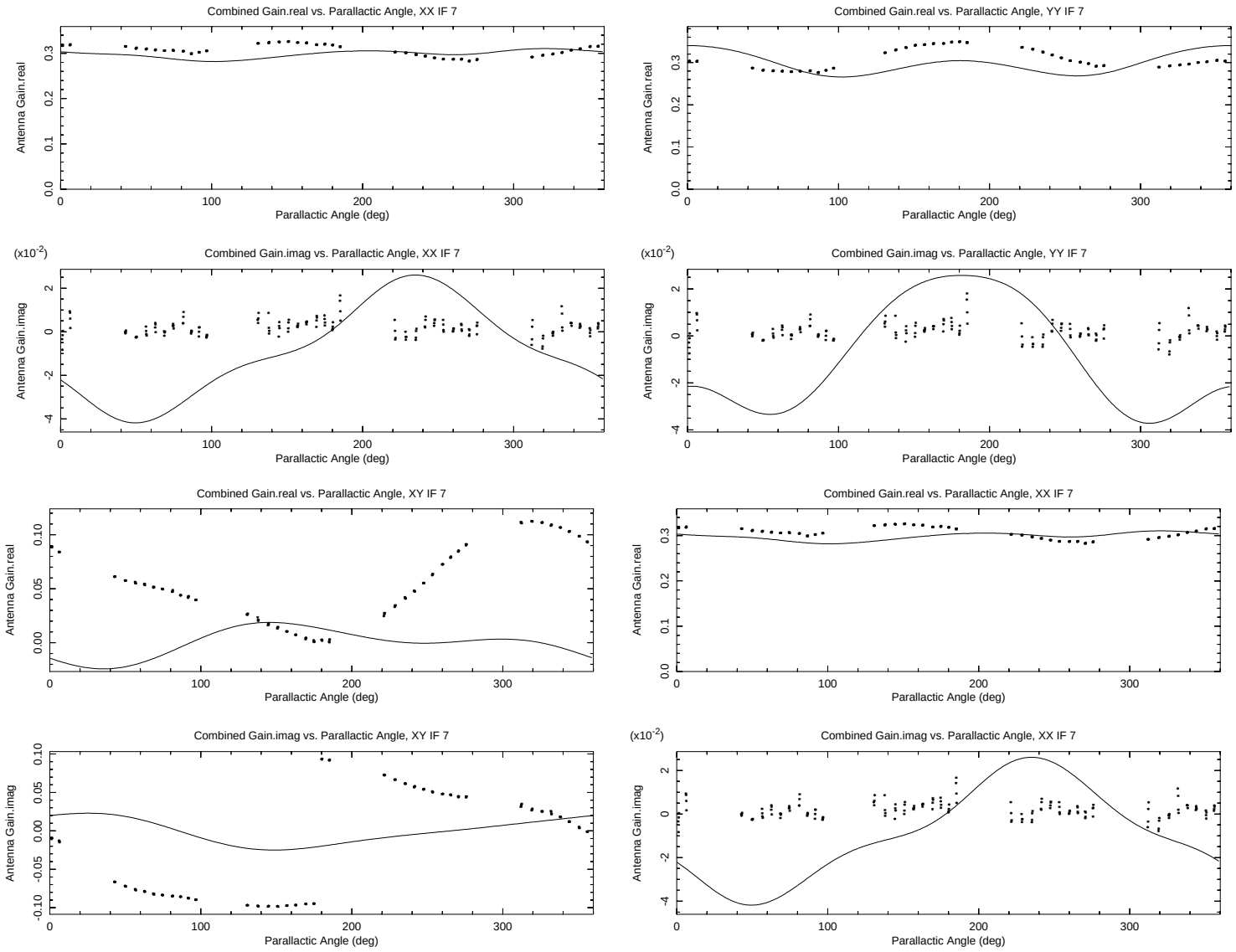

Fig. 5. XX,YY,XY and YX gains for Spectral Window 7 visibilities for all pointings. Like Figure 4 but for Spectral window 7.

In order to compare the model visibility shown in Figure 8 with the expected level seem in the beam holography images, a dataset was constructed by replacing the data with that expected from the calibrator polarization model (Fourier transform of the CLEAN components). The averaged visibilities as a function of parallactic angle is shown for one of the pointings in Figure 10 together with the interpolated holography beam values.

The XY and YX correlations are especially of interest, for a partially polarized point source and perfect feeds, they are relatively simple functions of Q, U, V and χ (parallactic angle) [12]:

$$XY = -Qsin(2\chi) + Ucos(2\chi) + j\ V$$
$$YX = -Qsin(2\chi) + Ucos(2\chi) - j\ V.$$

The real parts are the same function of linear polarization and the imaginary parts are $\pm$ the circular polarization. The XY and YX real parts seen in Figure 10 are of order 1% where as the imaginary parts are of order 0.1%.

The measured XY and YX correlations shown in Figure 7 are substantially larger than the CLEAN polarization model shown in Figure 10 so the latter are not dominated by the calibrator polarization. Additional evidence is that if the measured cross hand visibilities were dominated by calibrator polarization, the plots of the data points for the various pointing offsets would all have the same shape. Instead, they are quite different showing that the effects are related to where in the antenna pattern the source is viewed.

D. Ionospheric Faraday Rotation

One of the possible complications of measuring beam patterns is ionospheric Faraday rotation (IFR) which causes a rotation in the Q–U plane; the rotation is proportional to the wavelength squared of the radio emission and can be fitted to Q/U spectra. This effect can be seen in observations of 3C286 on 14 Aug 2022 in Figure 11. This effect should not be very prominent in observations of the very weakly polarized

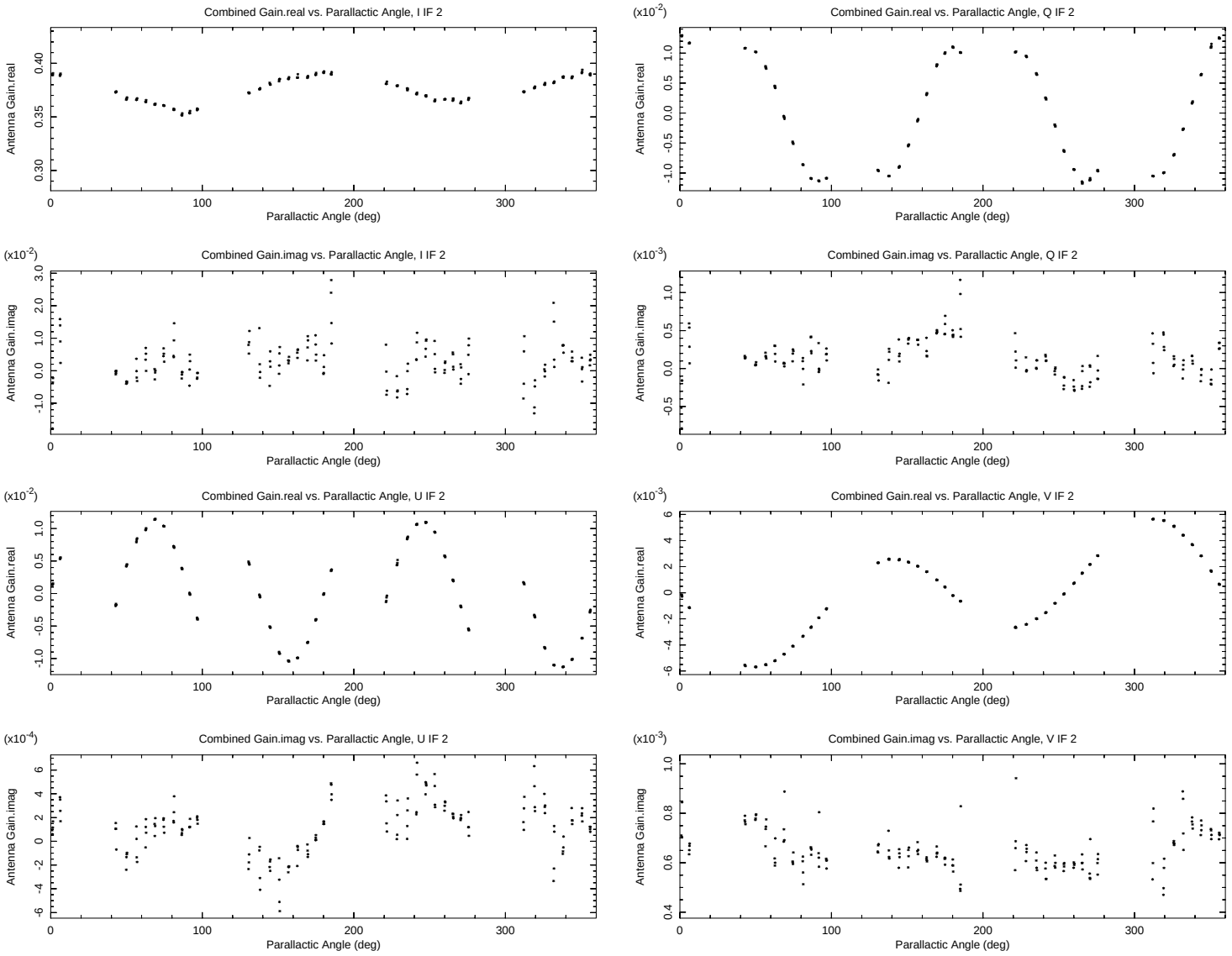

Fig. 6. I, Q, U and V gains from data for Spectral Window 2 visibilities for all pointings. Stars ("*") are 30 sec averages of visibilities over baseline and channel, normalised by the on–axis Stokes I flux density. Parallactic angles of data points are adjusted to include the effect of the direction of the position offset Upper panel real, lower imaginary.
Top Left: I
Top Right: Q
Bottom Left: U
Bottom Right: V

calibrator PKS0408-65 as there is little linear polarisation to rotate. However, the polarized calibrator 3C138 was observed twice in the 14 June 2023 and can be used to test for IFR. As can be seen from Figure 12, there is little evidence for this effect in this dataset.

III. Discussion

The results in Section II are difficult to understand. The measured correlations when the calibrator dominating the field is viewed off axis are not described by the measured beam holography. This is true with or without on–axis polarization calibration. The discrepancy is not due to the low (but detectable) level of linear polarization in the calibrator. Differing sign conventions do not appear to be the issue. Antenna gains derived from observing a calibrator off–axis using reference pointing give absolute values in the cross–hand gains substantially in excess of the expected values from the beam holography; this is especially true of the imaginary parts. Ionospheric Faraday rotation does not appear to be a problem in the 14 June 2023 data.

IV. Acknowledgment

I would like to thank the South African Radio Astronomy Observatory (SARAO) for access to the reference point test data and especially to Ludwig Swardt and Tom Mauch for making the observations and adjustments to the software.

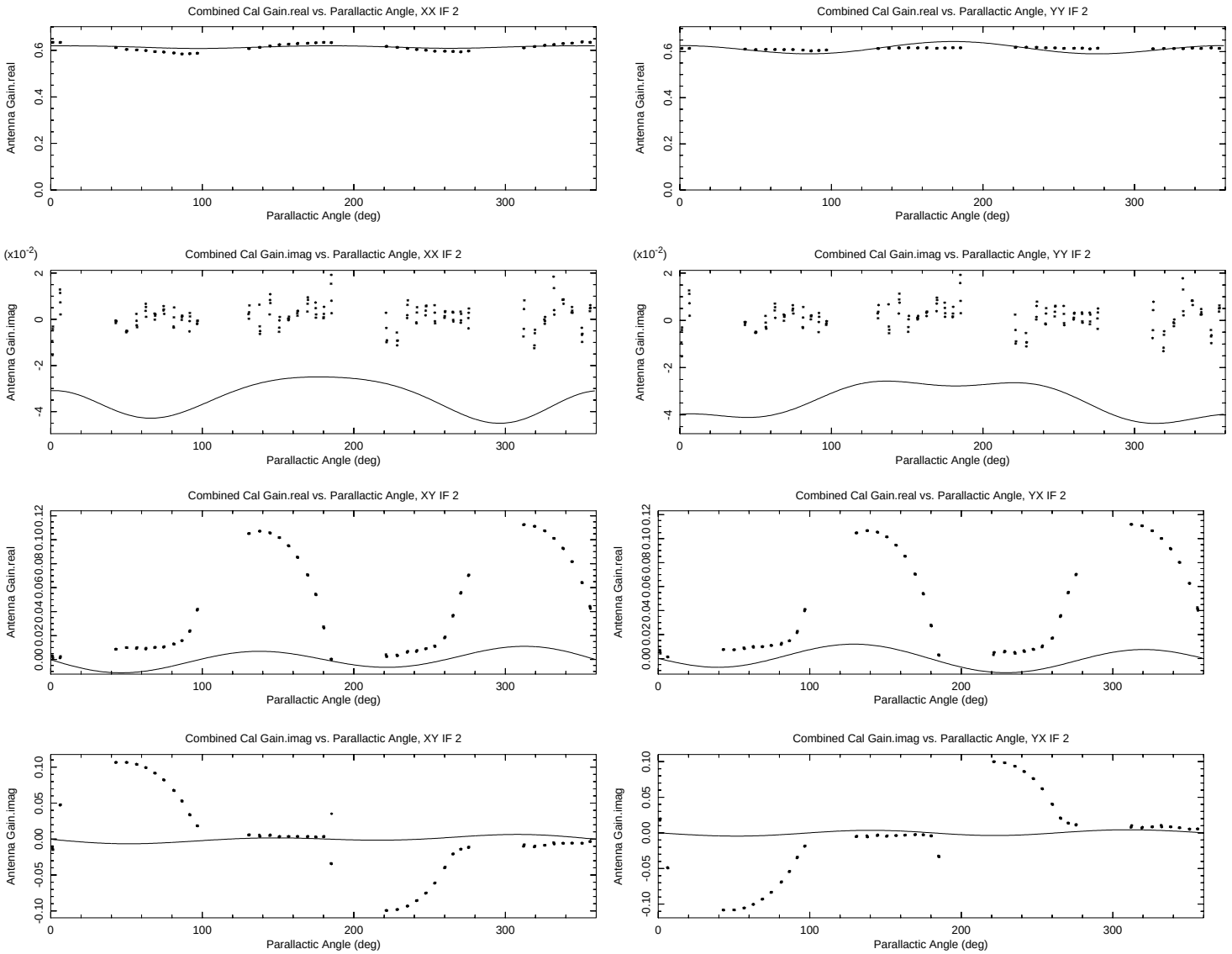

Fig. 7. XX,YY,XY and YX gains from polarization calibrated data for Spectral Window 2 visibilities for all pointings. Stars ("*") are 30 sec averages of visibilities over baseline and channel, normalised by the on–axis flux density. Parallactic angles of data points are adjusted to include the effect of the direction of the position offset The solid line is Mattieu de Villiers's antenna beam model [8] interpolated to the corresponding beam location and frequency. These are plotted over the full range of parallactic angle.
Upper panel real, lower imaginary.
Top Left: XX
Top Right: YY
Bottom Left: XY
Bottom Right: YX

REFERENCES

[1] W. D. Cotton and R. Perley, "EVLA Off-axis Beam and Instrumental Polarization," *Obit Development Memo Series*, vol. 17, pp. 1–22, 2010. [Online]. Available: https://www.cv.nrao.edu/∼bcotton/ObitDoc/EVLABeam.pdf

[2] ——, "EVLA Beam Holography take 2," *Obit Development Memo Series*, vol. 47, pp. 1–13, 2017. [Online]. Available: https://www.cv.nrao.edu/∼bcotton/ObitDoc/EVLABeam17.pdf

[3] W. D. Cotton and T. Mauch, "Beam Corrections and Heterogeneous Arrays I: Total Intensity," *Obit Development Memo Series*, vol. 70, pp. 1–, 2020. [Online]. Available: https://www.cv.nrao.edu/∼bcotton/ObitDoc/HeteroArray.pdf

[4] ——, "Beam Corrections and Heterogeneous Arrays II: Polarization," *Obit Development Memo Series*, vol. 71, pp. 1–, 2021. [Online]. Available: https://www.cv.nrao.edu/∼bcotton/ObitDoc/HeteroArrayPol.pdf

[5] ——, "Correction of Radio Interferometric Imaging for Antenna Patterns," *PASP*, vol. 133, no. 1028, p. 104502, Oct. 2021.

[6] W. D. Cotton, "Obit: A Development Environment for Astronomical Algorithms," *PASP*, vol. 120, pp. 439–448, 2008.

[7] M. S. de Villiers and W. D. Cotton, "MeerKAT Primary-beam Measurements in the L Band," *AJ*, vol. 163, no. 3, p. 135, Mar. 2022.

[8] M. S. de Villiers, "MeerKAT Holography Measurements in the UHF, L, and S Bands," *AJ*, vol. 165, no. 3, p. 78, Mar. 2023.

[9] J. J. Condon, W. D. Cotton, S. V. White, S. Legodi, S. Goedhart, K. McAlpine, S. M. Ratcliffe, and F. Camilo, "Threads, Ribbons, and Rings in the Radio Galaxy IC 4296," *ApJ*, vol. 917, no. 1, p. 18, Aug. 2021.

[10] W. D. Cotton, "Averaging over Baseline with Position Shift," *Obit Development Memo Series*, vol. 78, pp. 1–2, 2023. [Online]. Available: https://www.cv.nrao.edu/∼bcotton/ObitDoc/AvgBL.pdf

[11] ——, "Polarization Calibration of Linear Feeds Keeping Linear Feed

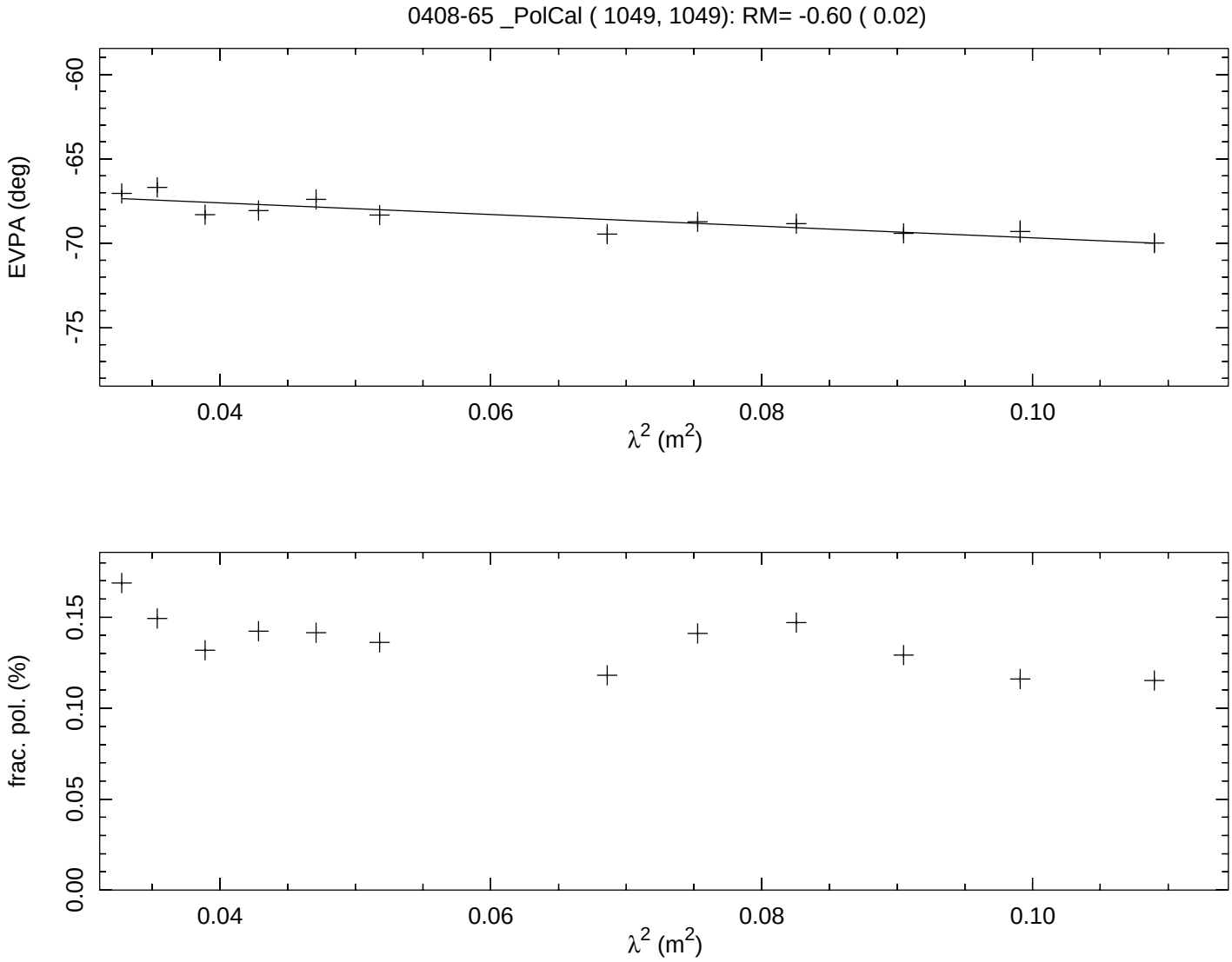

Fig. 8. Polarization spectrum of 0408-65. Subband RMSes are shown as error bars.
Upper: EVLA as a function of λ^2, Pluses (+) are subband averages and the line is the fitted RM.
Lower: Fractional polarization as a function of λ^2.

Basis," *Obit Development Memo Series*, vol. 81, pp. 1–5, 2023. [Online]. Available: https://www.cv.nrao.edu/∼bcotton/ObitDoc/LinPolCal.pdf

[12] A. R. Thompson, J. M. Moran, and G. W. Swenson, Jr., *Interferometry and Synthesis in Radio Astronomy, 2nd Edition*, Thompson, A. R., Moran, J. M., & Swenson, G. W., Jr., Ed. Wiley-Interscience, 2001.

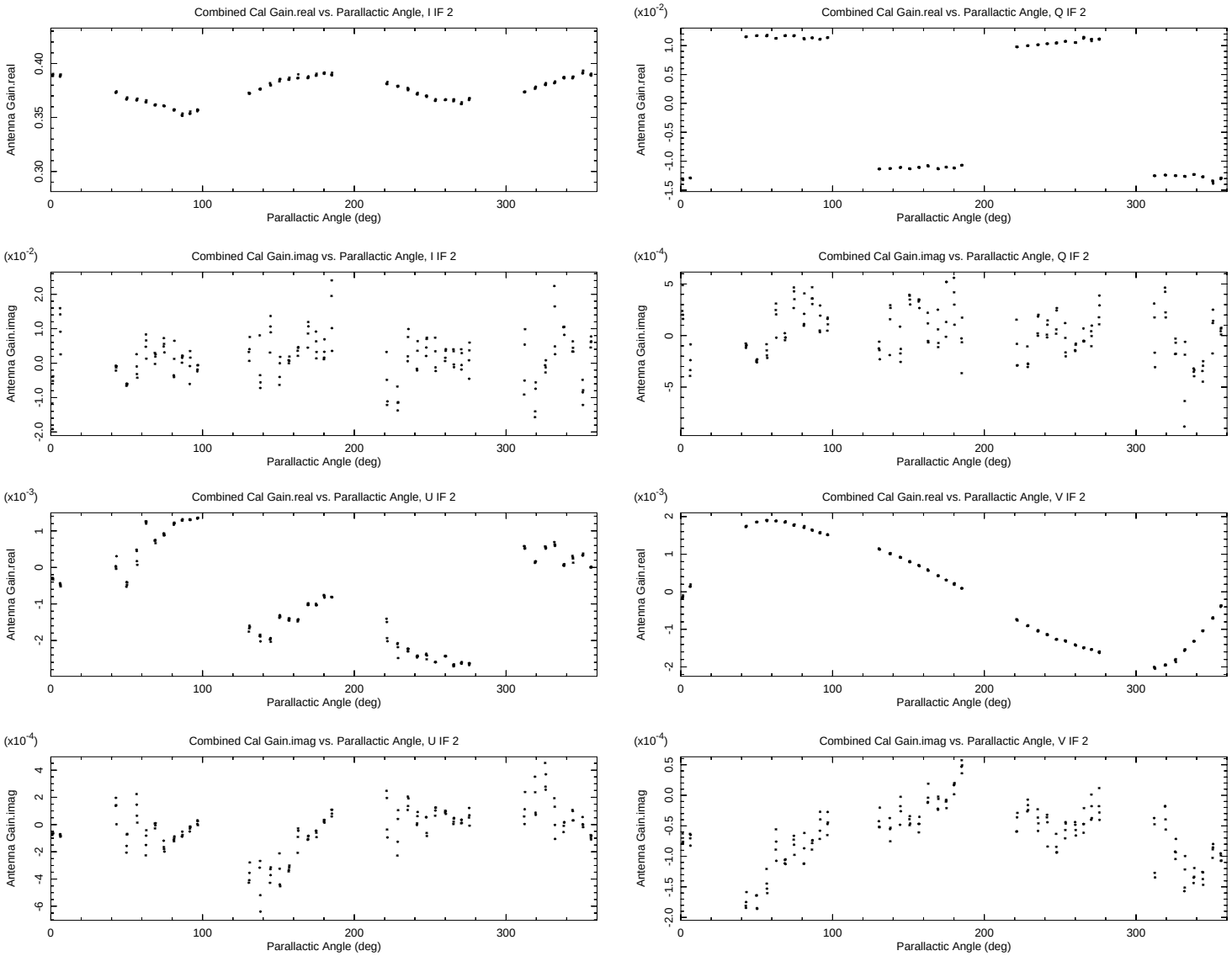

Fig. 9. I, Q, U and V gains from polarization calibrated data for Spectral Window 2 visibilities for all pointings. Stars ("*") are 30 sec averages of visibilities over baseline and channel, normalised by the on–axis flux density. Parallactic angles of data points are adjusted to include the effect of the direction of the position offset Upper panel real, lower imaginary.
Top Left: I
Top Right: Q
Bottom Left: U
Bottom Right: V

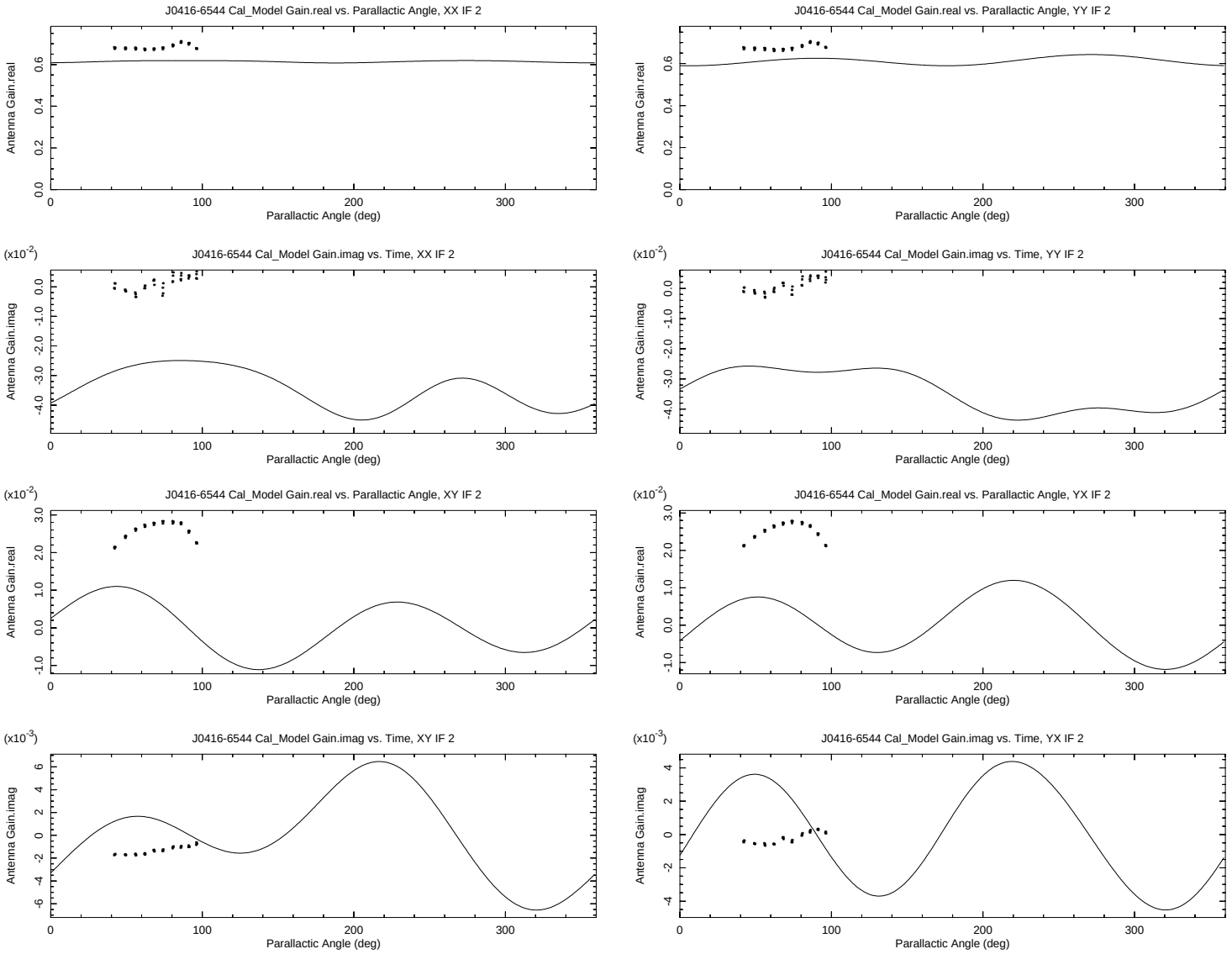

Fig. 10. Model visibilites of 0408-65 ("+") shown in Figure 8 as a function of parallactic angle for IF2.
The solid line is the antenna beam model interpolated to the corresponding beam location and frequency for pointing J0408-5455.
Top Left: XX
Top Right: YY
Bottom Left: XY
Bottom Right: YX

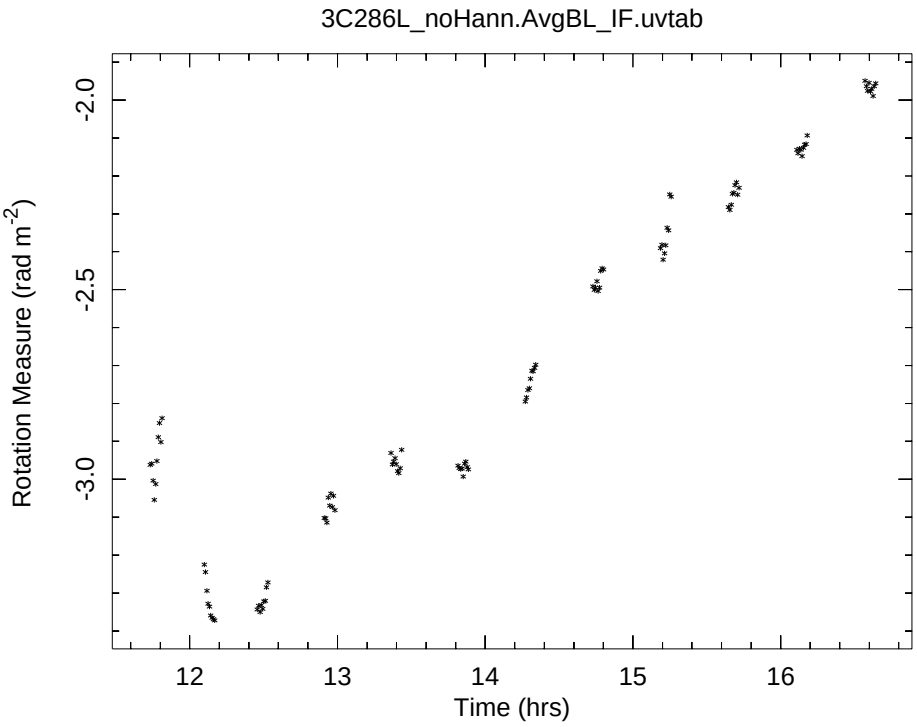

Fig. 11. Thirty second averages of Faraday rotation as a function of time on 3C286 on 14 Aug 2022 showing a change in the ionospheric Faraday rotation.

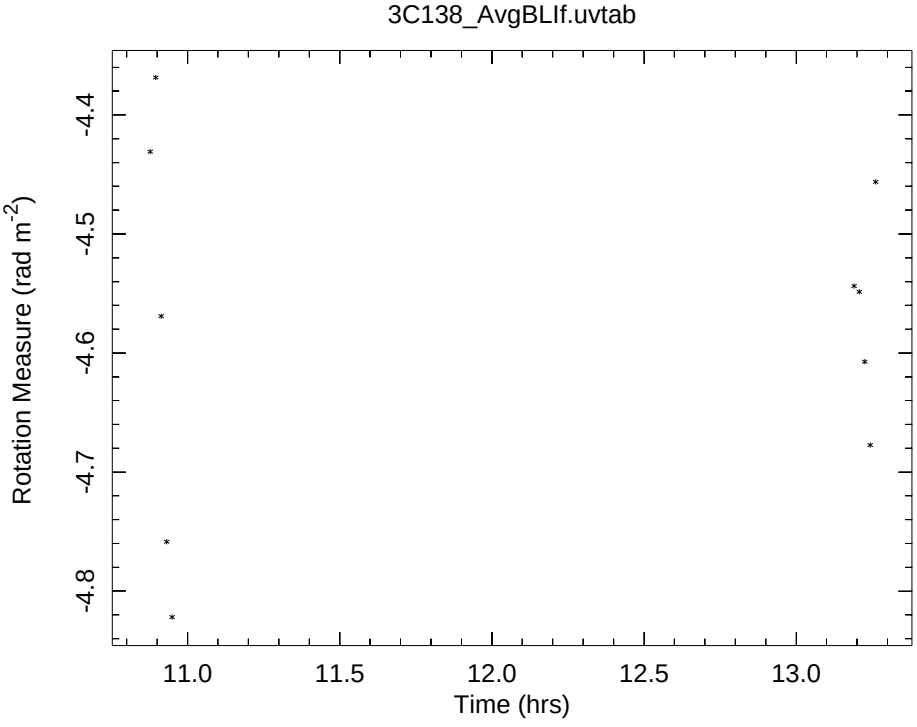

Fig. 12. One minute averages of the Faraday rotation as a function of time on 3C138 on 14 June 2023 showing no change in the ionospheric Faraday rotation.